MAGNETIC RESONANCE IN MEDICINE

Dynamic Changes in Water ADC, Energy Metabolism, Extracellular Space Volume, and Tortuosity in Neonatal Rat Brain During Global Ischemia

Annette van der Toorn, Eva Syková, Rick M. Dijkhuizen, Ivan Voříšek, Lydia Vargová, Evan Škobisová, Menno van Lookeren Campagne, Torsten Reese, Klaas Nicolay

To obtain a better understanding of the mechanisms underlying early changes in the brain water apparent diffusion coefficient (ADC) observed in cerebral ischemia, dynamic changes in the ADC of water and in the energy status were measured at postnatal day 8 or 9 in neonatal rat brains after cardiac arrest using ^{1}H MRS/MRI and ^{31}P MRS, respectively. The time courses of the MR parameters were compared with changes in the extracellular space (ECS) volume fraction (α) and tortuosity (λ), determined from concentration-time profiles of tetramethylammonium applied by iontophoresis. The data show a decrease of the ADC of tissue water after induction of global ischemia of which the time course strongly correlates with the time course of the decrease in the ECS volume fraction and the increase in ECS tortuosity. This indicates that cell swelling is an important cause for the ADC decrease of water.

Key words: diffusion, tortuosity, global ischemia, rat brain

INTRODUCTION

In the past few years, diffusion-weighted ^{1}H MRI and MRS have become increasingly important for assessing several different brain pathologies. Decreases of the apparent diffusion coefficient (ADC) of water have been observed in the early stages of ischemia (1–8), in status epilepticus (9), upon injection of excitotoxic stimuli (10–12), and during spreading depression (13).

Cell swelling caused by cytotoxic edema is proposed to cause the ADC reduction in early cerebral ischemia (5). Busza *et al.* (1) showed that changes in the intensity of diffusion-weighted images occur at blood flow values that are known to cause energy depletion and membrane depolarization (14), which are processes connected with cytotoxic cell swelling. In a model of *N*-methyl-D-aspartate (NMDA)-induced brain injury in neonatal rats, Verheul *et al.* (12) recently showed that the time course of excitotoxin-induced cell swelling, estimated from electrical impedance measurements, closely correlated with the time course of water ADC reduction. A similar correlation was noticed upon renormalization of the ADC and cell volume as brought about by NMDA antagonists (12). Therefore, it appears that the above NMDA- and NMDA-antagonist-induced changes in brain water ADC are caused either by changes in the volume fraction and/or diffusion properties of the extracellular space (ECS), by changes in the volume fraction and/or diffusion properties of the intracellular compartment, or by a combination of these effects.

Diffusion in the ECS can be studied by observing the diffusion of exogenous substances to which cell membranes are relatively impermeable, e.g., tetramethylammonium (TMA) ions. Diffusion in the ECS obeys Fick's law with two important modifications (15, 16). First, molecules in the ECS diffuse only through a restricted volume of the tissue, i.e., through the extracellular space volume fraction (α). The effective concentration of a diffusing substance is therefore higher than it would have been in a free medium (15). Secondly, the diffusion coefficient, D, is reduced by the square of the tortuosity (λ) to an apparent diffusion coefficient $D^* = D/\lambda^2$, because the diffusing substance encounters membrane obstructions, glycoproteins, macromolecules of the extracellular matrix, etc. Therefore, λ represents the increased path length for diffusion between two points. In addition to these two geometrical factors, diffusion in the ECS is affected by nonspecific uptake k', the factor describing the loss of material across the cell membranes (15, 17). The three diffusion parameters of the ECS (i.e., α, λ, and k') and their dynamic changes can be studied in vivo by the real-time iontophoretic method (15), which uses ion-selective microelectrodes to follow the diffusion of an extracellular marker (e.g., TMA) applied by iontophoresis. The TMA method has been used previously to measure changes in the ECS diffusion parameters of rat brain caused by acute and chronic ischemia (18, 19). In the early phase of ischemia, the ECS volume fraction decreases and the tortuosity increases (18). By contrast, the chronic phase of ischemic brain injury is accompanied by an increase of the ECS volume fraction and a decrease in the tortuosity (19).

MRM 36:52–60 (1996)

From the Department of in vivo NMR, Bijvoet Center for Biomolecular Research, Utrecht University, Utrecht, The Netherlands (A.T., R.M.D., T.R., K.N.); the Laboratory of Cellular Neurophysiology, Institute of Experimental Medicine ASCR, Prague, Czech Republic (E.S., I.V., L.V., E.S.); the Department of Neurosurgery, University Hospital Utrecht, Utrecht, The Netherlands (R.M.D.); the Third Medical Faculty, Charles University, Prague, Czech Republic (L.V.); and the Netherlands Institute of Brain Research, Amsterdam, The Netherlands (M.L.C.).

Address correspondence to: Annette van der Toorn, Ph.D., Department of Molecular Physics, Agricultural University Wageningen, Transitorium, Dreyenlaan 3, 6703 HA Wageningen, The Netherlands.

Received June 21, 1995; revised December 29, 1995; accepted January 26, 1995.

The NMR part of this work was conducted at the Netherlands *in vivo* NMR facility at the Bijvoet Center for Biomolecular Research, which is supported by the Netherlands Organization for Scientific Research (NWO). T.R. was a research fellow of the (European Union) Human Capital and Mobility program while these studies were performed. The *in vivo* measurements of diffusion parameters by the TMA^+ method were supported by Grant GA CR No. 309/93/1048, Grant GA CR No. 309/94/1107, and U.S.-Czech Science and Technology Program Award No. 92048.

Present address (M.L.C.): F. Hoffmann-La Roche Ltd., PRPN, Bau 69/402, Grenzacherstrasse 124, CH-4002, Basel, Switzerland.

0740-3194/96 $3.00

The objective of this investigation was to study the relationship between changes in water ADC, tissue energy status and extracellular space diffusion parameters in a model of global ischemia in neonatal rat brain. Global ischemia was induced by cardiac arrest (20) and may serve as a model for early cerebral ischemia. Brain water ADC was measured with ^{1}H MRS and MRI, and the energy status of the tissue was deduced from ^{31}P MRS measurements. The MR data were compared with measurements of extracellular space volume fraction (α), tortuosity (λ), and nonspecific uptake (k') by analyzing tetramethylammonium ion (TMA^+) diffusion curves in the extracellular space.

MATERIALS AND METHODS

NMR

All NMR measurements were performed on a SISCO (Spectroscopy Imaging Systems Corporation, Fremont, CA) 4.7 T NMR system. Wistar rats, 8–9 days of age, were anesthetized with urethane (3.2 g/kg ip). Body temperature was maintained at 37°C throughout all experiments with heating pads. After positioning the animals for the NMR measurements, a needle was inserted intraperitoneally to enable injection of salt solutions from outside the magnet, i.e., saturated KCl, inducing cardiac arrest or 0.9% w/v NaCl as a control. In all cases, the start of the ip injection is defined as time zero.

Diffusion-weighted MRS of the brain water was performed using the stimulated echo acquisition mode sequence (21, 22) with a shielded gradient set (maximum 18 mT/m). The rat head was put in a solenoidal coil with two turns and a diameter of 3 cm. A cubic volume of interest (VOI) of 132 μl was positioned centrally in the brain, guided by MR images. The VOI comprised approximately 75% of the brain. Diffusion weighting was accomplished by inserting diffusion weighting gradients in the z direction (perpendicular to the long axis of the animal) during the two *TE* delays. The measurements were performed with a diffusion gradient duration (δ) of 17 ms, a delay between the two diffusion weighting gradients (Δ) of 301 ms, and six different gradient amplitudes (b values 472, 734, 969, 1238, 1435, 1874 s/mm^2; *TE* 45 ms; TM 280 ms; *TR* 2 s; four acquisitions). This series of measurements (48 s each) was repeated for about 45 min. Injection of 1.5 ml of saturated KCl (n = 8) or physiological (0.9% w/v) NaCl (n = 2) was started after the fifth ADC measurement and took about 80 s. The exact moment of cardiac arrest could not be determined, so the start of the injection was set to time 0 min. After calculating the absolute value spectrum, the ADC and the S_0 (the integral of the water peak without diffusion weighting) were obtained by fitting the integrals of the water peak to the Stejskal-Tanner equation (23):

$$S = S_0 e^{-bADC} \qquad [1]$$

Where S is the measured signal integral and b is the b value ($b = \gamma^2 G^2 \delta^2 (\Delta - \delta/3)$, where γ is the gyromagnetic ratio and G is the used gradient strength). If the quality of the fit was not according to the preset standards ($R > 0.97$ and error $< 0.1^{*}10^{-3}$ mm^2/s), macroscopic motion was assumed and the measurement was discarded.

Diffusion-prepared U-FLARE (Ultrafast Low Angle RARE [Rapid Acquisition with Relaxation Enhancement]) imaging (24) was used to obtain spatially resolved ADC data (n = 4). A gradient insert with gradients up to 100 mT/m was used. Diffusion weighting was accomplished using diffusion-weighting gradients in the z direction (i.e., perpendicular to the image slice) around the 180° pulse during the preparation part of the experiment (δ 12 ms, Δ 18 ms, 10 b values ranging up to 1500 s/mm^2, *TE* 40 ms, slice thickness 2.5 mm). In the U-FLARE imaging part, 64 phase encoding steps were used and stepped from low to high spatial frequencies. Four scans were accumulated with a *TR* of 2.18 s, thus leading to a total time of 87 s per series of 10 b values. ADC maps were calculated by fitting the intensities of the images to the Stejskal-Tanner equation (Eq. [1]) on a pixel-by-pixel basis.

^{31}P MR spectra were measured with a pulse-acquire experiment, using a surface coil (single turn, 1.5 cm diameter) for signal restriction. A square pulse was used, which was calibrated for maximum signal yield from inorganic phosphate (P_i), at the repetition time used (*TR* 1.1 s, 108 acquisitions). Five spectra were acquired before ip injection of saturated KCl (n = 8) or 0.9% w/v NaCl (n = 4), after which acquisition was continued for about 40 min. The metabolites in the ^{31}P spectra were quantified using MINIVARPRO (provided by Dr. R. de Beer, Delft University of Technology, Delft, The Netherlands). This time-domain fitting program fitted the amplitudes of the metabolites using fixed damping constants of 50 Hz for ATP and PCr and of 70 Hz for P_i and PME (phosphomonoesters), based on linewidths estimated from spectra taken under control conditions. Furthermore, the chemical shifts of the ATP and PCr resonances were fixed, whereas the chemical shifts of P_i and PME were allowed to change. Signal amplitudes were normalized by dividing by the initial PCr amplitude. The PCr resonance was set at 0 ppm. The pH of the tissue was calculated from the chemical shift of the P_i peak relative to that of PCr (δP_i) according to the relationship (Eq. [2]) used by Remy *et al.* (25):

$$\mathrm{pH} = 6.66 + \log((\delta P_i - 3.079)/(5.57 - \delta P_i)) \qquad [2]$$

Measurements of ECS Diffusion Parameters

Experiments were performed on 11 Wistar rat pups 8–10 days of age. Animals were anesthetized with urethane 1.6–3.2 g/kg ip. The animals spontaneously breathed air during the experiments. A hole, 2–3 mm in diameter, was made over the somatosensory neocortex and the dura was carefully removed. The exposed brain cortex was bathed in warmed artificial cerebrospinal fluid. The fluid and body temperatures were recorded and maintained at 37°C. Cardiac arrest was induced by injecting saturated KCl or $MgCl_2$ in a similar procedure as used for the NMR experiments. Saturated $MgCl_2$ was used in some cases to establish that injected K^+ did not significantly change the measurements. No significant differences were found between both methods.

Ion-selective microelectrodes (ISMs) were used to measure TMA^+ diffusion parameters in ECS. Double-barreled ISMs for TMA^+ were made as described elsewhere (26). The ion exchanger was Corning 477317 and the ion-sensing barrel was backfilled with 100 mM tetramethylammonium chloride (TMA chloride), and the reference barrel contained 150 m*M* NaCl. The electrodes were calibrated using the fixed-interference method before and after each experiment in a series of flowing solutions of 150 m*M* NaCl + 3 m*M* KCl with the addition of the following amounts of TMA chloride (m*M*): 0.0003, 0.001, 0.003, 0.01, 0.03, 0.1, 0.3, 1.0, 3.0, 10.0. Calibration data were fitted to the Nikolsky equation to determine electrode sensitivity and interference (26).

For TMA^+ diffusion measurements, iontophoresis pipettes were prepared from theta glass. The shank was bent before backfilling with 1 M TMACl, so that it could be aligned parallel to that of the ISM. Electrode arrays were made by gluing together an iontophoresis pipette and a TMA^+ selective microelectrode with tip separation of 130–200 μm (Fig. 1). Typical iontophoresis parameters were 20 nA bias current (continuously applied to maintain a constant transport number) and +80 nA current step with 60 s duration to generate the diffusion curve. TMA^+ diffusion curves were captured on a digital oscilloscope (Nicolet 3091, Nicholet Instrument Corporation, Madison, WI) and then transferred to a 486 computer, on which they were analyzed by fitting the data to a solution of the diffusion equation (see below) using the program VOLTORO (C. Nicholson, unpublished).

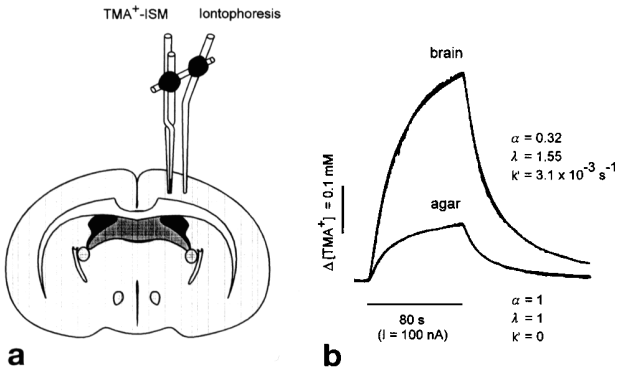

FIG. 1. Method of determining the ECS volume fraction (α), tortuosity (λ), and nonspecific uptake (k') in rat brain in vivo. (a) Schematic drawing of the experimental arrangement for diffusion measurements. Two microelectrodes, the double-barreled TMA^+ selective microelectrode (TMA^+-ISM) and micropipette for TMA^+ iontophoresis, were glued together with dental cement at their upper ends to stabilize the intertip distance (typically 80–200 μm). (b) Typical diffusion curves obtained in agar and brain. Measurements in agar (whereby definition $\alpha = 1$, $\lambda = 1$, $k' = 0$) enabled the transport number of the iontophoretics electrode to be determined. The iontophoretic current, applied as pulses of 80 s duration, was 100 nA. When the electrode array was lowered into the rat brain and the same iontophoretic current was applied, the resulting increase in concentration was much larger than that in agar because of the restricted volume fraction ($\alpha = 0.32$) and increased tortuosity ($\lambda = 1.55$). The nonspecific uptake was $k' = 3.1 \times 10^{-3}\ s^{-1}$. In this figure, the TMA^+ concentration scale is linear and the theoretical diffusion curve, calculated from Eqs. [3] and [4] (see Methods), is superimposed on each experimental curve.

TMA^+ concentration versus time curves were first recorded in 0.3% agar gel (Special Noble Agar, Difco, Detroit, MI) made up in 150 m*M* NaCl, 3 m*M* KCl and 0.3 m*M* TMA^+ in a Lucite cup that could be placed just above the brain. The array of electrodes was then lowered into the brain for 900 μm, to reach the cortical lamina V (grey matter) and for 1700 μm to reach white matter tissue (corpus callosum) (27). The position relative to bregma was 2–3 mm anterior-posterior and 2–3 mm laterally from midline. The diffusion curves obtained were analyzed to yield the extracellular volume fraction α, the tortuosity λ, and the nonspecific, concentration-dependent uptake term, k' (s^{-1}). These three parameters were extracted by a nonlinear curve fitting simplex algorithm operating on the diffusion curve described by Eqs. [3] and [4]:

$$G(u) = (Q\lambda^2/8\pi\Delta\alpha r) \times \{exp[r\lambda(k'/D)^{1/2}]erfc[r\lambda/2(Du)^{1/2} + (k'u)^{1/2}] + exp[-r\lambda(k'/D)^{1/2}]erfc[r\lambda/2(Du)^{1/2} - (k'u)^{1/2}]\} \quad [3]$$

$$C(t) = G(t) \quad \text{for the rising phase of the curve, } t < S, \quad [4a]$$

$$C(t) = G(t) - G(t - S) \quad \text{for the falling phase of the curve, } t > S, \quad [4b]$$

The quantity of TMA^+ delivered to the tissue per second is $Q = In/zF$, where I is the step increase in current applied to the iontophoresis electrode, n is the transport number, z is the number of charges associated with the substance iontophoresed (here +1), and F is Faraday's electrochemical equivalent. The function "*erfc*" is the complementary error function.

In equation [3], $G(u)$ represents the time dependence of the TMA^+ concentration at distance r from the source electrode. It is assumed that TMA^+ diffuses out from the source electrode with spherical symmetry and that the iontophoresis current is applied for duration S. Then, the rising phase of the measured TMA^+ concentration ($C(t)$) curve (that is, at $t < S$) can be evaluated by substituting t for u in Eq. [3]. The falling phase of the measured TMA^+ concentration curve (that is, at $t > S$) can be evaluated by using the substitution shown in equation [4b].

For agar as experimental medium, α and λ are, by definition, set to 1 and k' is set to be 0, whereas the parameters n and D are extracted by curve fitting. Knowing n and D, the parameters α, λ, and k' can be obtained when the experiment is repeated in the brain.

Results of the experiments were expressed as the mean ± SEM. Statistical analysis of the differences between groups (injected with saturated $KCl/MgCl_2$ (n = 15) or with 0.9% NaCl (n = 2)) was evaluated by one-way analysis of variance (ANOVA) test. Values of $P < 0.05$ were considered significant. In six cases, the temporal development of the ECS diffusion parameters was fol-

lowed in white matter after inducing cardiac arrest, and in five cases, similar measurements were performed in grey matter.

RESULTS

Changes in Brain Water ADC as Induced by Cardiac Arrest

Changes in the brain water ADC as observed with localized MRS are shown in Fig. 2. The control ADC as measured before injection of KCl was $0.92 \pm 0.02 \times 10^{-3}$ mm^2/s (mean ± SEM, $n = 8$). This seems to be a very high value for the ADC in rat brain. However, the ADC in neonatal rat brain is higher than the ADC observed in adult rat brain, because the extracellular space volume in neonatal rat brain is much higher than that of adult rat brain (27). Because the ADC of extracellular water is probably higher than the ADC of intracellular water, changes in the ratios between them will cause changes in the overall ADC observed for water. The increased extracellular volume fraction of neonatal rats will therefore be accompanied by a higher water ADC compared to adult rat brain.

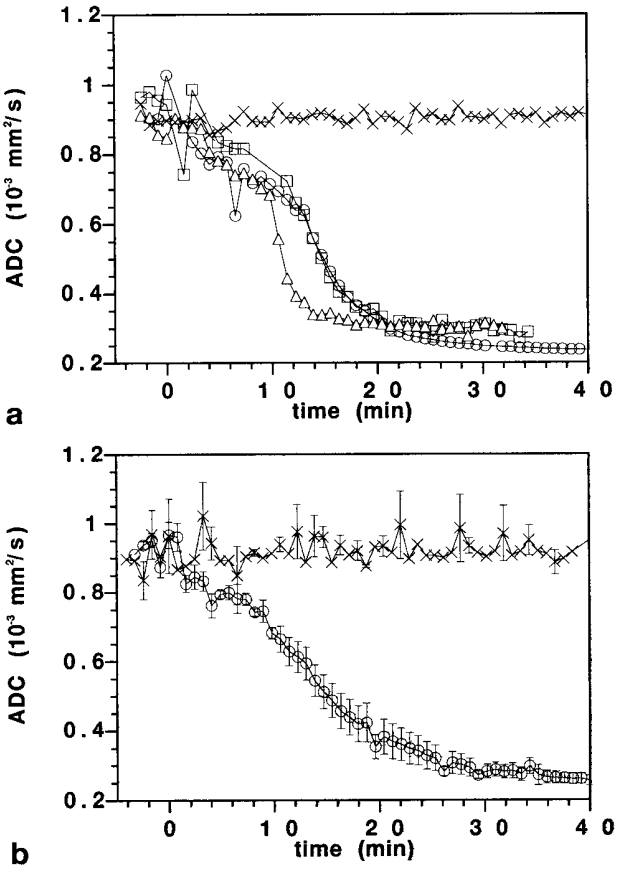

FIG. 2. Changes in the ADC measured with diffusion-weighted localized ^1H MRS (132 μl) in typical individual rats (a) and averaged over all rats (b) upon induction of cardiac arrest by injection of saturated KCl (○, △, and □ in (a) and ○, $n = 9$ in (b)) or after injection with physiological NaCl (X, with $n = 3$ in (b)). The injection took place at time 0 min. Data points in (b) depict mean ± SEM.

The ADC decreased in two distinct phases after KCl injection, which was used to induce cardiac arrest (Fig. 2B). Initially, the ADC decreased slowly at a rate of about 0.01 to 0.02×10^{-3} mm^2/s per minute. After about 8–10 min this was followed by a phase in which the ADC decreased more rapidly, i.e., at a rate of about 0.03 to 0.05 $\times 10^{-3}$ mm^2/s per min. Approximately 20–30 min after KCl injection, the ADC stabilized at $0.26 \pm 0.02 \times 10^{-3}$ mm^2/s. Figure 2A shows that the temporal pattern differed somewhat among individual animals. This is probably caused by variations in the time that cardiac arrest occurred and/or metabolic differences between the animals. The control group, which was injected with 0.9% w/v NaCl, did not suffer cardiac arrest and subsequent ischemia, and the brain water ADC remained unchanged.

Diffusion-prepared U-FLARE MR imaging was used to monitor the water ADC changes in a spatially resolved manner. Potential regional differences in the response could thus be observed. A representative series of ADC maps before and after cardiac arrest is shown in Fig. 3. ADC maps were measured at a similar anterior-posterior position as used for the ECS and tortuosity measurements. Figure 4 depicts the mean ADC for three different regions in the rat brain: white matter, basal ganglia, and cortical grey matter. The regions of interest for white matter and cortical grey matter were chosen to coincide with the electrode positions used in the TMA^+ diffusion measurements. In the first 5–10 min after injection of KCl, the ADC decreased slowly in all regions. This was followed by a period of rapid ADC reduction. Finally, stabilization of the ADC occurred after 20–30 min. Interestingly, the time courses of the ADC decrease varied with brain region. The phase of rapid ADC reduction was initiated considerably earlier in grey matter than in white

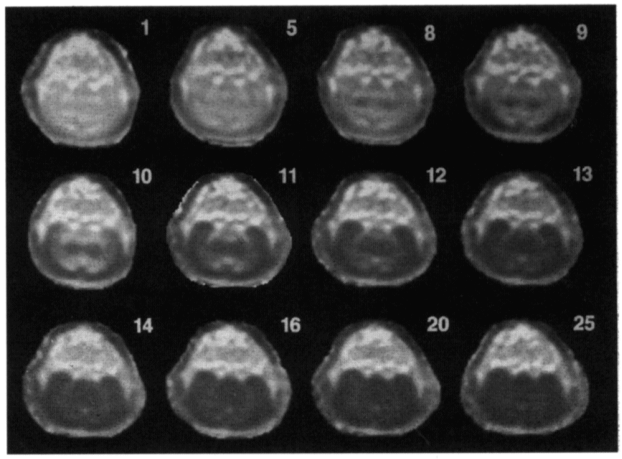

FIG. 3. Water ADC maps of a representative neonatal rat brain at different times after injection of saturated KCl, inducing cardiac arrest. The maps depict the calculated ADC on a pixel-by-pixel basis. The ADC was calculated using diffusion-weighted images obtained with U-FLARE (10 *b* values ranging up to 1500 s/mm^2) and fitting the intensities of corresponding pixels in the images to Eq. [1]. A total of 25 maps were acquired (87 s each). Numbers refer to: control image (1), start of KCl injection (5), and approximately 4.5 min (8), 5.5 min (9), 7 min (10), 8.5 min (11), 10 min (12), 11.5 min (13), 13 min (14), 16 min (16), 22 min (20), and 29 min (25) after KCl injection.

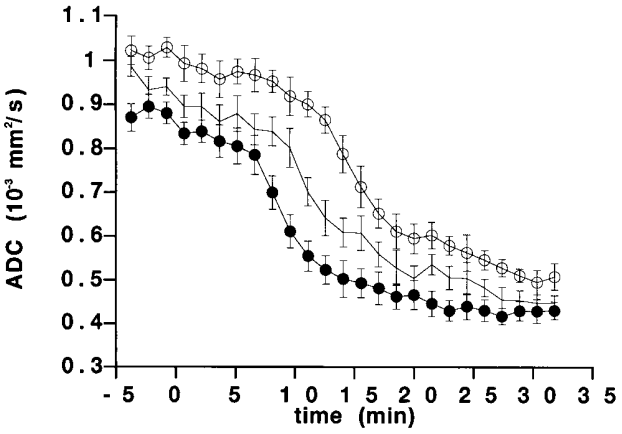

FIG. 4. Regional changes in the ADC measured with diffusion-weighted U-FLARE in the rat brain upon induction of cardiac arrest by injection of saturated KCl (n = 4). ADC analysis was done in white matter (○), grey matter (●) and basal ganglia (no symbol). Data points depict mean ± SEM.

matter. This might be because of the differences in susceptibility to ischemia of these tissues.

^{31}P Magnetic Resonance Spectroscopy Measurements

^{31}P MRS was used to assess the energetic status of the neonatal brain tissue in relation to the induction of global ischemia. Representative ^{31}P spectra taken at various time points before and after KCl injection are shown in Fig. 5. The time-dependent changes can be directly compared with the ADC changes measured with diffusion-weighted MRS, because in both cases, the response was averaged over almost the whole brain. The signal intensities of P_i, PCr, and γ-ATP averaged over all observed animals are shown in Fig. 6 (a, b, and c, respectively). Figure 6d depicts the time course of changes in tissue pH. After KCl injection, a decrease of the PCr and the ATP peaks was observed, paralleled by an increase in the P_i peak together with a decrease in the intracellular pH. The

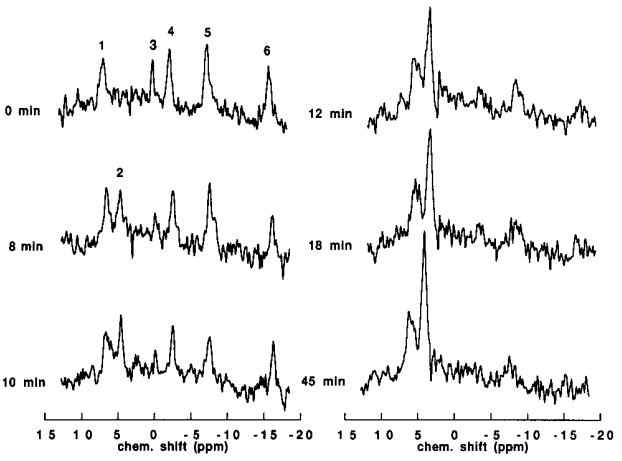

FIG. 5. ^{31}P spectra obtained from neonatal rat brain upon injection of saturated KCl (starting at 0 min) and subsequent global ischemia. 1: phosphomonoesters (PME); 2: P_i; 3: PCr; 4: γ-ATP; 5: α-ATP; 6: β-ATP.

PCr resonance decreased at a higher rate than the ATP resonances. PCr was virtually depleted after approximately 12 min. After about 30 min, no more changes were observed in the spectra. No significant changes were observed in the PME resonance (data not shown). In control experiments, in which the animals were injected with physiological NaCl, no significant changes in the ^{31}P spectra were observed (Fig. 6).

Extracellular Space Volume Fraction and Tortuosity

In parallel experiments, the diffusion of TMA^+ was studied in cortical layer V (at a depth of 700–900 μm from the dorsal surface of the brain) and in subcortical white matter (at a depth of 1500–1700 μm) (27) before and after cardiac arrest. The TMA^+ diffusion gives spatially localized information about changes in the extracellular space diffusion parameters — the extracellular volume fraction α, the tortuosity λ, and the nonspecific TMA^+ uptake k'. Figure 7 shows a typical experiment in grey matter (lamina V), in which TMA^+ diffusion curves were recorded before and during ischemia. A slow increase of the TMA^+ baseline was observed in the first 10 min after KCl injection, and a relatively fast increase was observed from 10 to 25 min. The increase was caused by an increase in base-line TMA^+ concentration due to extracellular space volume shrinkage (20 nA bias current was continuously applied throughout the experiment; see also Methods). The TMA^+ diffusion curves were superimposed on this baseline throughout the experiment. As ischemia progressed, the amplitude of the curves increased (note that the y axis has a logarithmic scaling). Two TMA^+ diffusion curves, one before and one after ischemia, are displayed with a linear scaling in Fig. 8, along with the values for the extracellular volume fraction α, the tortuosity λ, and the nonspecific uptake k' as obtained by fitting the experimental data to Eq. [3]. The TMA^+ diffusion curve reached a higher amplitude in anoxic brain tissue because of a decrease of the extracellular volume.

Figure 9 shows the time courses (mean ± SEM) of changes in α, λ, and k' evoked by global ischemia in grey matter (n = 5) and in white matter (n = 6). After injection of KCl, a decrease in the volume fraction α and increase in the tortuosity were observed, both in grey and in white matter. After 20–30 min, the extracellular volume fraction and the tortuosity in grey matter stabilized at about 0.05 ± 0.01 (mean ± SEM, n = 5) and 2.07 ± 0.08, respectively. It is evident that the changes in extracellular space diffusion parameters were slower in white matter than in lamina V of the cortical grey matter. Table 1 shows that no statistically different values of α, λ, and k' were found in the cortex and white matter after ischemia, whereas α and k′ were significantly higher in the white matter before ischemia (27). The experiments on rats injected with NaCl showed no significant changes in the ECS diffusion parameters (data not shown). Concomitantly with the decrease in α and the increase in λ, the nonspecific uptake k' significantly increased. However, the k' values remained relatively low during ischemia (Fig. 9).

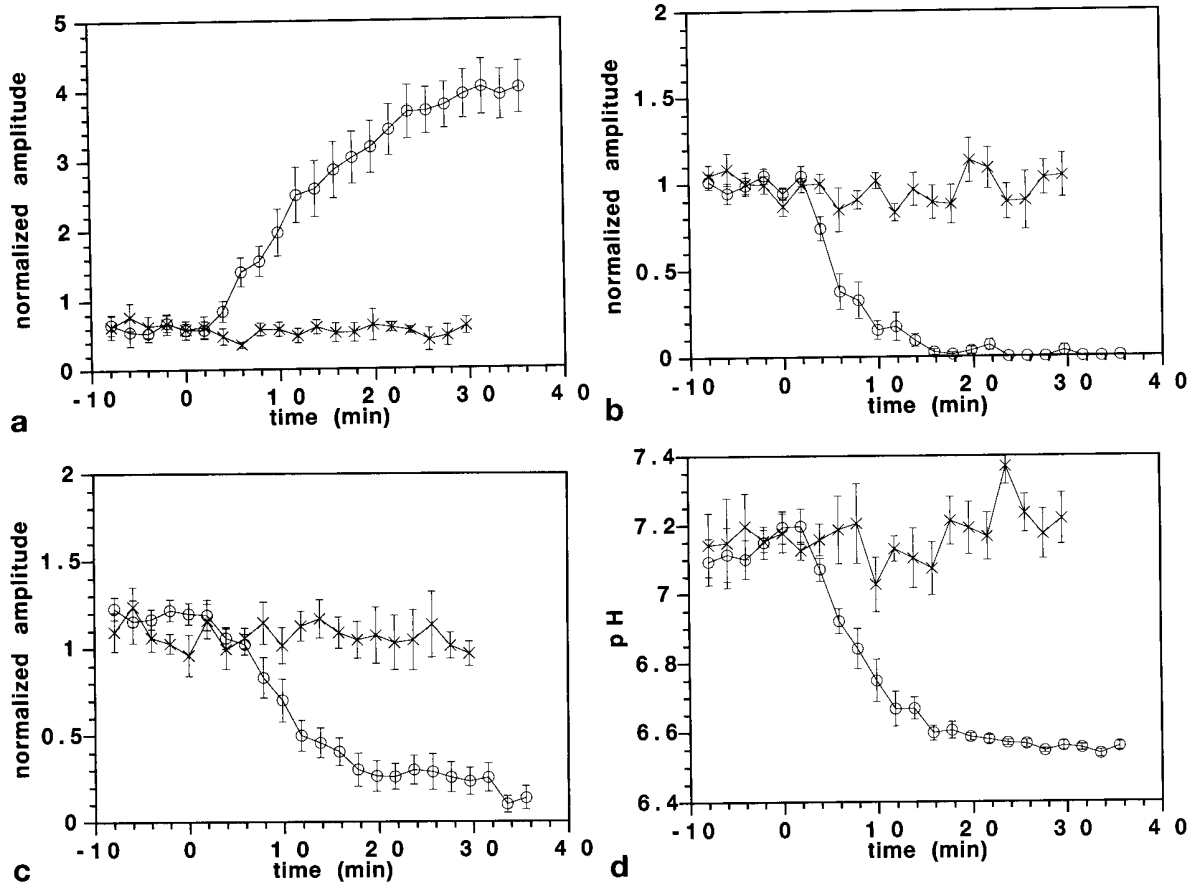

FIG. 6. Averaged changes in normalized signal amplitudes of P_i (a), PCr (b), and γ-ATP (c), as well as of the pH (d) upon injection of saturated KCl (○, n = 8) or physiological NaCl (X, n = 4). Signal amplitudes were obtained by time domain fitting of ^{31}P spectra. Signal amplitudes were normalized by dividing by the PCr amplitude measured before injection of salt solutions. Data points depict mean ± SEM.

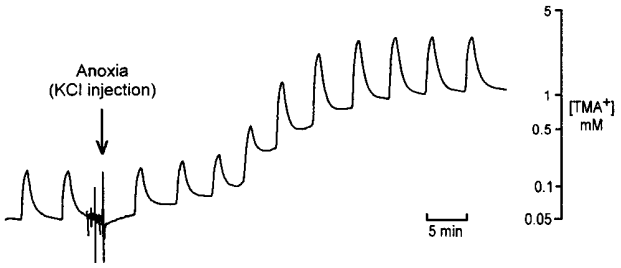

FIG. 7. Typical TMA^+ diffusion experiment in cortical grey matter (lamina V) of a 9-day-old rat. The TMA^+ diffusion curves were recorded before and during global ischemia evoked by ip injection of KCl. The TMA^+ base-line increases and the superimposed diffusion curves show an increasing amplitude as ischemia progresses, because the scaling is logarithmic.

DISCUSSION

Our studies on the effects of global ischemia in neonatal rat brain show that there is a close correlation between the time course of the decrease in the ADC of brain water observed with NMR (Figs. 2 and 4) and the time course of changes in the ECS volume fraction and the tortuosity, as obtained by the TMA^+ method (Fig. 9). This strongly suggests that the changes in the parameters mentioned above are all mechanistically linked to the same ischemia-induced processes. The observed decrease in the ECS volume fraction and the increase in ECS tortuosity imply that cell swelling occurred. Therefore, the concomitant ADC decrease presumably is also caused by cell swelling. It should be noted that water rapidly exchanges across cell membranes and thus may reflect diffusion in both the intra- and extracellular space. Consequently, the observed water ADC changes may result from changes in the extracellular and/or intracellular compartments.

Time course correlations are particularly evident when comparing changes in the water ADC (Fig. 4) to changes in the ECS volume fraction and tortuosity in different brain regions (Fig. 9). ADC changes occur later after induction of ischemia in white matter than in grey matter. This difference is also manifest in the ECS volume fraction and tortuosity measurements for grey and white matter. Such regional differences are indicative of variations in susceptibility to ischemia, a phenomenon that has been noted in several other studies (28, 29).

Our experiments also revealed a time-course correlation between changes in the diffusion parameters detected by NMR and TMA^+ methods and changes in the energy status, as determined with ^{31}P MRS (Fig. 6). A few minutes after KCl injection, the PCr peak started to decrease, along with with an increase in the P_i peak and a

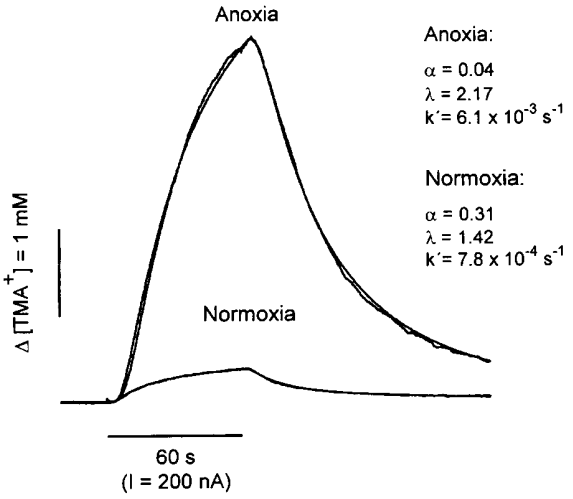

FIG. 8. TMA^+ diffusion curves recorded in cortical grey matter (lamina V) before (normoxia) and after global ischemia (anoxia) induced by ip injection of $MgCl_2$ in 8-day-old rat. The concentration scale is linear and the theoretical diffusion curve (Eq. [3]) is superimposed on each data curve. The diffusion curve after ischemia is much higher than in normal conditions because of the lower volume fraction α (ischemic 0.04, normal 0.31), the higher tortuosity λ (ischemic 2.17, normal 1.42), and a slightly changed k' (ischemic 0.0061 s^{-1}, normal 0.00078 s^{-1}).

decreasing pH. The ATP resonance started to decline somewhat later and more slowly than the PCr resonance. This phenomenon has also been shown in several models of temporary ischemia (14, 30). It indicates that the cells are trying to maintain a constant ATP concentration through the creatine kinase reaction while consuming PCr. Interestingly, the start of the rapid decrease in the water ADC (Fig. 2) coincides with the time that PCr has been depleted (Fig. 6). After about 30 min, no further changes in the ^{31}P spectra were observed, while the ADC also stabilized. It is more difficult to compare the ^{31}P data with data on the ECS parameters, because the ^{31}P spectra are a weighted average of signals from both white and grey matter. Nevertheless, our data suggest that PCr depletion represents an important triggering point for the initiation of massive cell swelling. The observed regional differences in the response of the water ADC and ECS parameters may thus be caused by differences in the time point of PCr depletion, as brought about by differences in the balance between free-energy use and delivery.

A model can be postulated that accounts for the time correlation between the decrease in the extracellular volume fraction, the increase in the tortuosity, and the compromised energy status. After induction of cardiac arrest, the glucose and oxygen supply to the brain stops, causing the tissue to switch to anaerobic glycolysis. When the ATP concentration has dropped below a certain threshold value, the cells lose the ability to maintain their membrane potential. Because of the stagnation of the Na^+/K^+ ATPase, Na^+ and Cl^- then leak into the cells and K^+ leaks out (31), leading to an osmotically obliged uptake of water that causes the cells to swell. This phenomenon is known as cytotoxic edema. Approximately 20–30 min after the induction of cardiac arrest, no further cell swelling occurred, as indicated by the stabilization of the ECS parameters. The cells have largely depleted their energy reserves by that time.

The water ADC changed in a biphasic manner (Figs. 2 and 4). Immediately after induction of cardiac arrest, the water ADC started to decrease slowly, followed by a fast decrease starting after 7–12 min. Although the temporal resolution of the ECS measurements is lower, a slow change in the ECS parameters could sometimes be observed in this period as well (Fig. 9). Both the ECS volume fraction and the tortuosity seem to change slowly in the first 10 min after induction of ischemia (Fig. 9). This suggests that a certain degree of cell swelling may be taking place before PCr has been depleted, presumably driven by K^+ accumulation (32).

A number of theories have been suggested to explain why cell swelling is accompanied by ADC changes. The most common one supposes that there is a fast exchange between water in the extracellular space and in the intracellular compartment and that, therefore, the measured ADC is a weighted average of both fractions (5). The ADC of water will decrease in the case of cytotoxic cell swelling because water moves from the extracellular space, where it has a high ADC, into the intracellular compartment, where the ADC of water has been demonstrated to be lower (33). In this model, it is usually assumed that the ADCs of water in both compartments do not change significantly with cell swelling. However, cell volume changes may modify both the intracellular and the extracellular water ADC. The TMA^+ diffusion experiments show that the extracellular diffusion can be significantly affected by changes in ECS geometry, represented here by extracellular space volume and tortuosity (Eq. [3]), which change when cytotoxic edema develops. Extracellular water probably also experiences an increasing tortuosity. The change in the ADC of the extracellular water fraction can be calculated using the equation $D^* = D/\lambda^2$, assuming: (1) that extracellular water *in vivo* has the same diffusion coefficient as free water at 37°C ($3 \cdot 10^{-3}$ mm^2/s (34)), (2) that the cell membrane is impermeable to water, and (3) that the same tortuosity values apply for water as for TMA^+. In this case, the extracellular water diffusion may decrease from $1.32 \cdot 10^{-3}$ mm^2/s to $0.69 \cdot 10^{-3}$ mm^2/s. Although the tortuosity factor for water may be different from that measured for TMA^+, it has been shown by Nicholson and Tao (16) that the tortuosity varies only slightly for molecules below a molecular weight range of 10–40 kDa. Therefore, it seems plausible that the change in the overall ADC of tissue water is not only caused by changes in the volume fractions of intracellular and extracellular water but also because the ADC of the extracellular fraction changes because of an increase in tortuosity after cytotoxic cell swelling. This notion is confirmed by findings of Latour *et al.* (35), who noticed that the ADC of water in a model system of packed red blood cells depended on the extracellular water fraction. The effect of cell swelling on the intracellular water ADC is unknown.

Additional mechanisms involved in the ADC changes cannot be excluded. There might be changes in the membrane permeability, which can cause the diffusion coefficient to change as proposed by Helpern *et al.* (36).

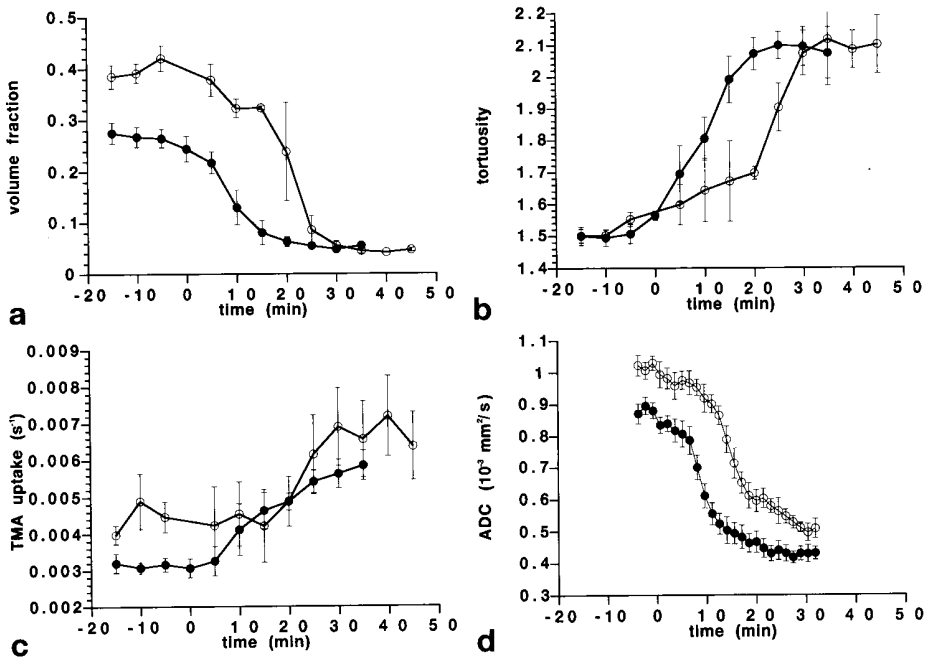

FIG. 9. Changes in the extracellular space volume fraction, α (a), the tortuosity λ (b), the nonspecific TMA^+ uptake k' (c), and the ADC (d) in the neonatal rat brain after injection of saturated KCl or $MgCl_2$ at $t = 0$. The extracellular space volume fraction α, the tortuosity λ, the nonspecific TMA^+ uptake k' were measured by the TMA^+ method; the ADC was obtained using U-FLARE imaging. Symbols: (●) grey matter; (○) white matter. Data points depict mean ± SEM ($n = 6$ white matter, $n = 5$ grey matter).

Table 1
Changes in the Extracellular Space Volume Fraction (α), Tortuosity (λ) and Nonspecific Uptake (k') Before (Normal) and Approximately 30 Minutes after Induction of Global Ischemia (ischemia).

	Gray matter		White matter	
	Normal	Ischemia	Normal	Ischemia
α (−)	0.27 ± 0.02	0.05 ± 0.005	0.40 ± 0.02	0.04 ± 0.002
λ (−)	1.50 ± 0.03	2.10 ± 0.06	1.52 ± 0.02	2.10 ± 0.05
k' (10^{-3} s^{-1})	3.2 ± 0.2	5.6 ± 0.3	4.4 ± 0.3	6.9 ± 0.1

Values are displayed as mean ± SEM ($n = 15$).

Although the data on the nonspecific uptake of TMA^+ suggest that there are significant changes in the membrane permeability, it is unknown whether and how the permeability of the cell membranes to water is modified.

In conclusion, this study shows that the changes in the ADC of brain tissue water, as induced by cardiac arrest and measured by diffusion-weighted in vivo MR techniques, predominantly report on cell volume changes. It seems likely that this correlation also applies to the early phase of other brain pathologies that are accompanied by cytotoxic cell swelling, including focal ischemia.

ACKNOWLEDGMENTS

The authors thank Dr. R. de Beer (Delft University of Technology, Delft, The Netherlands) for use of MINIVARPRO to fit the ^{31}P spectra and Prof. C. Nicholson (New York University Medical Center, New York, NY) for use of the VOLTORO program.

REFERENCES

1. A. L. Busza, K. L. Allen, M. D. King, N. Van Bruggen, S. R. Williams, D. G. Gadian, Diffusion-weighted imaging studies of cerebral ischemia in gerbils. *Stroke* **23,** 1602–1612 (1992).
2. D. Davis, J. Ulatowski, S. Eleff, M. Izuta, S. Mori, D. Shungu, P. C. M. Van Zijl, Rapid monitoring of changes in water diffusion coefficients during reversible ischemia in cat and rat brain. *Magn. Reson. Med.* **31,** 454–460 (1994).
3. R. A. Knight, R. J. Ordidge, J. A. Helpern, M. Chopp, L. C. Rodolosi, D. Peck, Temporal evolution of ischemic damage in rat brain measured by proton nuclear magnetic resonance imaging. *Stroke* **22,** 802–808 (1991).
4. J. Kucharczyk, J. Mintorovitch, H. S. Asgari, M. E. Moseley, Diffusion/perfusion MR imaging of acute cerebral ischemia. *Magn. Reson. Med.* **19,** 311–315 (1991).
5. M. E. Moseley, Y. Cohen, J. Mintorovitch, L. Chileuitt, H. Shimizu, J. Kucharczyk, M. F. Wendland, P. R. Weinstein, Early detection of regional cerebral ischemia in cats: comparison of diffusion- and T2-weighted MRI and spectroscopy. *Magn. Reson. Med.* **14,** 330–346 (1990).
6. M. J. Quast, N. C. Huang, G. R. Hillman, T. A. Kent, The evolution of acute stroke recorded by multimodal magnetic resonance imaging. *Magn. Reson. Imaging* **11,** 465–471 (1993).
7. T. P. L. Roberts, A. Vexler, N. Derugin, M. E. Moseley, J. Kucharczyk, High-speed MR imaging of ischemic brain injury following stenosis of the middle cerebral artery. *J. Cereb. Blood Flow Metab.* **13,** 940–946 (1993).
8. P. Van Gelderen, M. H. M. De Vleeschouwer, D. DesPres, J. Pekar, P. C. M. Van Zijl, C. T. W. Moonen, Water diffusion and acute stroke. *Magn. Reson. Med.* **31,** 154–163 (1994).
9. J. Zhong, O. A. C. Petroff, J. W. Prichard, J. C. Gore, Changes in water diffusion and relaxation properties of rat cerebrum during status epilepticus. *Magn. Reson. Med.* **30,** 241–246 (1993).
10. M. Van Lookeren-Campagne, J. B. Verheul, K. Nicolay, R. Balazs, Terminal evolution of NMDA-induced excitotoxicity in the neonatal rat brain measured with ^1H nuclear magnetic resonance imaging. *Brain Res.* **618,** 203–212 (1994).
11. H. B. Verheul, R. Balazs, J. W. Berkelbach van der Sprenkel, C. A. F. Tulleken, K. Nicolay, M. Van Lookeren Campagne, Temporal evolution of NMDA-induced excitotoxicity in the neonatal rat brain mea-

sured with 1H nuclear magnetic resonance imaging. *Brain Res.* **618,** 203–212 (1993).
12. H. B. Verheul, R. Balazs, J. W. Berkelbach van der Sprenkel, C. A. F. Tulleken, K. Nicolay, K. S. Tamminga, M. Van Lookeren Campagne, Comparison of diffusion-weighted MRI with changes in cell volume in a rat model of brain injury. *NMR Biomed.* **7,** 96–100 (1994).
13. L. L. Latour, Y. Hasegawa, J. E. Formato, M. Fisher, C. H. Sotak, Spreading waves of decreased diffusion coefficient after cortical stimulation in the rat brain. *Magn. Reson. Med.* **32,** 189–198 (1994).
14. K. L. Allen, A. L. Busza, E. Proctor, M. D. King, S. R. Williams, H. A. Crockard, D. G. Gadian, Controllable graded cerebral ischaemia in the gerbil: studies of cerebral blood flow and energy metabolism by hydrogen clearance and ^{31}P NMR spectroscopy. *NMR Biomed.* **6,** 181–186 (1993).
15. C. Nicholson, J. M. Phillips, Ion diffusion modified by tortuosity and volume fraction in the extracellular microenvironment of the rat cerebellum. *J. Physiol.* **321,** 225–257 (1981).
16. C. Nicholson, L. Tao, Hindered diffusion of high molecular weight compounds in brain extracellular microenvironment measured with integrative optical imaging. *Biophys. J.* **65,** 2277–2290 (1993).
17. C. Nicholson, Measurement of extracellular space, *in* "Practical Electrophysiological Methods: A Guide for In Vitro Studies in Vertebrate Neurobiology," (H. Kettermann, R. Grantyn, Eds.), pp. 367–372, Wiley, New York, 1992.
18. J. A. Lundbaek, A. J. Hansen, Brain interstitial volume fraction and tortuosity in anoxia. Evaluation of the ion-selective microelectrode method. *Acta. Physiol. Scand.* **146,** 473–484 (1992).
19. E. Syková, J. Svoboda, J. Polak, A. Chvatal, Extracellular volume fraction and diffusion characteristics during progressive ischemia and terminal anoxia in the spinal cord of the rat. *J. Cereb. Blood Flow Metab.* **14,** 301–311 (1994).
20. J. Korf, C. Klein, K. Venema, F. Postema, Increases in striatal and hippocampal impedance and extracellular levels of amino acids by cardiac arrest in freely moving rats. *J. Neurochem.* **50,** 1087–1096 (1988).
21. J. Frahm, K. -D. Merboldt, W. Hänicke, Localized proton spectroscopy using stimulated echoes. *J. Magn. Reson.* **72,** 502–508 (1987).
22. J. Granot, Selected volume excitation using stimulated echoes (VEST). Applications to spatially localized spectroscopy and imaging. *J. Magn. Reson.* **70,** 488–492 (1986).
23. E. O. Stejskal, J. E. Tanner, Spin diffusion measurements: spin echoes in the presence of a time-dependent field gradient. *J. Chem. Phys.* **42,** 288–292 (1965).
24. D. G. Norris, P. Börner, T. Reese, D. Leibfritz, On the application of ultrafast RARE experiments. *Magn. Reson. Med.* **27,** 142–164 (1992).
25. C. Remy, J. P. Albrand, A. L. Benabid, M. Decorps, M. Jacrot, J. Riondel, M. F. Foray, In vivo 31P nuclear magnetic resonance studies of T1 and T2 relaxation times in rat brain and in rat brain tumors implanted to nude mice. *Magn. Reson. Med.* **4,** 144–152 (1987).
26. C. Nicholson, M. E. Rice, Use of ion-selective micro-electrodes and voltametric microsensors to study brain cell microenvironment, *in* "Volume Transmission in the Brain, Novel Mechanisms for Neural Transmission," (K. Fluxe, L. F. Agnati, Eds.), p. 279–294, Raven Press, New York, 1988.
27. A. Lehmenkühler, E. Syková, J. Svoboda, K. Zilles, C. Nicholson, Extracellular space parameters in the rat neocortex and subcortical white matter during postnatal development determined by diffusion analysis. *Neuroscience* **55,** 339–351 (1993).
28. B. Bose, S. C. Jones, R. Lorig, H. T. Friel, M. Weinstein, J. R. Little, Evolving focal cerebral ischemia in cats; spatial correlation of nuclear magnetic resonance imaging, cerebral blood flow, tetrazolium staining, and histopathology. *Stroke* **19,** 28–37 (1988).
29. T. Higuchi, E. J. Fernandez, A. A. Maudsley, M. W. Weiner, Mapping of cerebral metabolites in rats by ^{1}H magnetic resonance spectroscopic imaging. *NMR Biomed.* **6,** 311–317 (1993).
30. L. -H. Chang, R. Shirane, P. R. Weinstein, T. L. James, Cerebral metabolite dynamics during temporary complete ischemia in rats monitored by time-shared 1H and 31P NMR spectroscopy. *Magn. Reson. Med.* **13,** 6–13 (1990).
31. K. -A. Hossmann, The pathophysiology of experimental brain edema. *Neurosurg. Rev.* **12,** 263–280 (1989).
32. E. Syková, Ionic and volume changes in the microenvironment of nerve and receptor cells, *in* "Progress in Sensory Physiology," (D. Ottoson, Ed.), pp. 1–167, Springer-Verlag, Heidelberg, 1992.
33. P. C. M. Van Zijl, C. T. W. Moonen, P. Faustino, J. Pekar, O. Kaplan, J. S. Cohen, Complete separation of intracellular and extracellular information in NMR spectra of perfused cells by diffusion-weighted spectroscopy. *Proc. Natl. Acad. Sci. U S A* **88,** 3228–3232 (1991).
34. D. Le Bihan, Molecular diffusion nuclear magnetic resonance imaging. *Magn. Reson. Q.* **7,** 1–30 (1991).
35. L. L. Latour, K. Svoboda, P. P. Mitra, C. H. Sotak, Time-dependent diffusion of water in a biological model system. *Proc. Natl. Acad. Sci. U S A* **91,** 1229–1233 (1994).
36. J. A. Helpern, R. J. Ordidge, R. A. Knight, The effect of cell membrane water permeability on the apparent diffusion coefficient of water, *in* "Proc., SMRM, 11th Annual Meeting," Berlin, 1992," p. 1201.